2

Low Sampling Rate Time Acquisition Schemes and Channel Estimation Algorithms of Ultra-Wideband Signals

Wei Xu and Jiaxiang Zhao
Nankai University
China

1. Introduction

Ultra-wideband (UWB) communication is a viable technology to provide high data rates over broadband wireless channels for applications, including wireless multimedia, wireless Internet access, and future-generation mobile communication systems (Karaoguz, 2001; Stoica et al., 2005). Two of the most critical challenges in the implementation of UWB systems are the timing acquisition and channel estimation. The difficulty in them arises from UWB signals being the ultra short low-duty-cycle pulses operating at very low power density. The Rake receiver (Turin, 1980) as a prevalent receiver structure for UWB systems utilizes the high diversity in order to effectively capture signal energy spread over multiple paths and boost the received signal-to-noise ratio (SNR). However, to perform maximal ratio combining (MRC), the Rake receiver needs the timing information of the received signal and the knowledge of the channel parameters, namely, gains and tap delays. Timing errors as small as fractions of a nanosecond could seriously degrade the system performance (Lovelace & Townsend, 2002; Tian & Giannakis, 2005). Thus, accurate timing acquisition and channel estimation is very essentially for UWB systems.

Many research efforts have been devoted to the timing acquisition and channel estimation of UWB signals. However, most reported methods suffer from the restrictive assumptions, such as, demanding a high sampling rates, a set of high precision time-delay systems or invoking a line search, which severally limits their usages. In this chapter, we are focusing on the low sampling rate time acquisition schemes and channel estimation algorithms of UWB signals. First, we develop a novel optimum data-aided (DA) timing offset estimator that utilizes only symbol-rate samples to achieve the channel delay spread scale timing acquisition. For this purpose, we exploit the statistical properties of the power delay profile of the received signals to design a set of the templates to ensure the effective multipath energy capture at any time. Second, we propose a novel optimum data-aided channel estimation scheme that only relies on frame-level sampling rate data to derive channel parameter estimates from the received waveform. The simulations are provided to demonstrate the effectiveness of the proposed approach.

2. The channel model

From the channel model described in (Foerster, 2003), the impulse response of the channel is

$$h(t) \quad = \quad X \sum_{n=1}^{N} \sum_{k=1}^{K(n)} \alpha_{nk} \delta(t - T_n - \tau_{nk}) \tag{1}$$

where X is the log-normal shadowing effect. N and $K(n)$ represent the total number of the clusters, and the number of the rays in the nth cluster, respectively. T_n is the time delay of the nth cluster relative to a reference at the receiver, and τ_{nk} is the delay of the kth multipath component in the nth cluster relative to T_n . From (Foerster, 2003), the multipath channel coefficient α_{nk} can be expressed as $\alpha_{nk} = p_{nk}\beta_{nk}$ where p_{nk} assumes either $+1$ or -1 with equal probability, and $\beta_{nk} > 0$ has log-normal distribution.
The power delay profile (the mean square values of $\{\beta_{nk}^2\}$) is exponential decay with respect to $\{T_n\}$ and $\{\tau_{nk}\}$, i.e.,

$$\langle \beta_{nk}^2 \rangle \quad = \quad \langle \beta_{00}^2 \rangle \exp(-\frac{T_n}{\Gamma}) \exp(-\frac{\tau_{nk}}{\gamma}) \tag{2}$$

where $\langle \beta_{00}^2 \rangle$ is the average power gain of the first multipath in the first cluster. Γ and γ are power-delay time constants for the clusters and the rays, respectively.
The model (1) is employed to generate the impulse responses of the propagation channels in our simulation. For simplicity, an equivalent representation of (1) is

$$h(t) \quad = \quad \sum_{l=0}^{L-1} \alpha_l \delta(t - \tau_l) \tag{3}$$

where L represents the total number of the multipaths, α_l includes log-normal shadowing and multipath channel coefficients, and τ_l denotes the delay of the lth multipath relative to the reference at the receiver. Without loss of generality, we assume $\tau_0 < \tau_1 < \cdots < \tau_{L-1}$. Moreover, the channel only allows to change from burst to burst but remains invariant (i.e., $\{\alpha_l, \tau_l\}_{l=0}^{L-1}$ are constants) over one transmission burst.

3. Low sampling rate time acquisition schemes

One of the most acute challenges in realizing the potentials of the UWB systems is to develop the time acquisition scheme which relies only on symbol-rate samples. Such a low sampling rate time acquisition scheme can greatly lower the implementation complexity. In addition, the difficulty in UWB synchronization also arises from UWB signals being the ultrashort low-duty-cycle pulses operating at very low power density. Timing errors as small as fractions of a nanosecond could seriously degrade the system performance (Lovelace & Townsend, 2002; Tian & Giannakis, 2005).
A number of timing algorithms are reported for UWB systems recently. Some of the timing algorithms(Tian & Giannakis, 2005; Yang & Giannakis, 2005; Carbonelli & Mengali, 2006; He & Tepedelenlioglui, 2008) involve the sliding correlation that usually used in traditional narrowband systems. However, these approaches inevitably require a searching procedure and are inherently time-consuming. Too long synchronization time will affect

symbol detection. Furthermore, implementation of such techniques demands very fast and expensive A/D converters and therefore will result in high power consumption. Another approach (Carbonelli & Mengali, 2005; Furusawa et al., 2008; Cheng & Guan, 2008; Sasaki et al., 2010) is to synchronize UWB signals through the energy detector. The merits of using energy detectors are that the design of timing acquisition scheme could benefit from the statistical properties of the power delay profile of the received signals. Unlike the received UWB waveforms which is unknown to receivers due to the pulse distortions, the statistical properties of the power delay profile are invariant. Furthermore, as shown in (Carbonelli & Mengali, 2005), an energy collection based receiver can produce a low complexity, low cost and low power consumption solution at the cost of reduced channel spectral efficiency.

In this section, a novel optimum data-aided timing offset estimator that only relies on symbol-rate samples for frame-level timing acquisition is derived. For this purpose, we exploit the statistical properties of the power delay profile of the received signals to design a set of the templates to ensure the effective multipath energy capture at any time. We show that the frame-level timing offset acquisition can be transformed into an equivalent amplitude estimation problem. Thus, utilizing the symbol-rate samples extracted by our templates and the ML principle, we obtain channel-dependent amplitude estimates and optimum timing offset estimates.

3.1 The signal model

During the acquisition stage, a training sequence is transmitted. Each UWB symbol is transmitted over a time-interval of T_{s} seconds that is subdivided into N_{f} equal size frame-intervals of length T_{f}. A single frame contains exactly one data modulated ultrashort pulse $p(t)$ of duration T_{p}. And the transmitted waveform during the acquisition has the form as

$$s(t) \quad = \quad \sqrt{E_{\mathrm{f}}} \sum_{j=0}^{NN_{\mathrm{f}}-1} d_{[j]_{N_{\mathrm{ds}}}} p(t - jT_{\mathrm{f}} - a_{\lfloor \frac{j}{N_{\mathrm{f}}} \rfloor} \triangle) \tag{4}$$

where $\{d_l\}_{l=0}^{N_{\mathrm{ds}}-1}$ with $d_l \in \{\pm 1\}$ is the DS sequence. The time shift $\triangle$ is chosen to be $T_{\mathrm{h}}/2$ with T_{h} being the delay spread of the channel. The assumption that there is no inter-frame interference suggests $T_{\mathrm{h}} \leq T_{\mathrm{f}}$. For the simplicity, we assume $T_{\mathrm{h}} = T_{\mathrm{f}}$ and derive the acquisition algorithm. Our scheme can easily be extended to the case where $T_{\mathrm{f}} \geq T_{\mathrm{h}}$. The training sequence $\{a_n\}_{n=0}^{N-1}$ is designed as

$$\{\underbrace{0,\, 0,\, 0,\, \cdots 0}_{n=0,1,\cdots,N_0-1}\ \underbrace{1,\, 0,\, 1,\, 0,\, \cdots 1,\, 0}_{n=N_0,N_0+1,\cdots,N-1}\}, \tag{5}$$

i.e., the first N_0 consecutive symbols are chosen to be 0, and the rest symbols alternately switch between 1 and 0.

The transmitted signal propagates through an L-path fading channel as shown in (3). Using the first arriving time τ_0, we define the relative time delay of each multipath as $\tau_{l,0} = \tau_l - \tau_0$

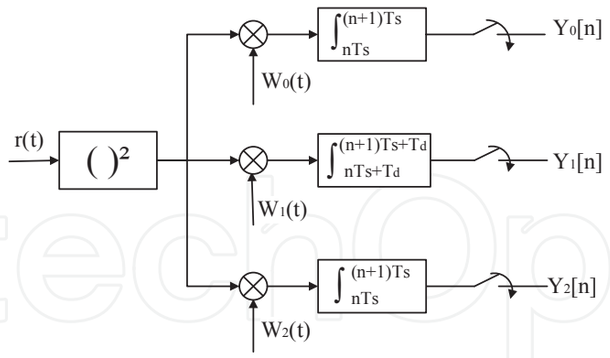

Fig. 1. The block diagram of acquisition approach.

for $1 \leq l \leq L-1$. Thus the received signal is

$$r(t) = \sqrt{E_{\mathrm{f}}} \sum_{j=0}^{NN_{\mathrm{f}}-1} d_{[j]_{N_{\mathrm{ds}}}} p_R(t - jT_{\mathrm{f}} - a_{\lfloor \frac{j}{N_{\mathrm{f}}} \rfloor} \Delta - \tau_0) + n(t) \tag{6}$$

where $n(t)$ is the zero-mean additive white Gaussian noise (AWGN) with double-side power spectral density $\sigma_n^2/2$ and $p_R(t) = \sum_{l=0}^{L-1} \alpha_l p(t - \tau_{l,0})$ represents the convolution of the channel impulse response (3) with the transmitted pulse $p(t)$.
The timing information of the received signal is contained in the delay τ_0 which can be decomposed as

$$\tau_0 \quad = \quad n_{\mathrm{s}} T_{\mathrm{s}} + n_{\mathrm{f}} T_{\mathrm{f}} + \xi \tag{7}$$

with $n_{\mathrm{s}} = \lfloor \frac{\tau_0}{T_{\mathrm{s}}} \rfloor$, $n_{\mathrm{f}} = \lfloor \frac{\tau_0 - n_{\mathrm{s}} T_{\mathrm{s}}}{T_{\mathrm{f}}} \rfloor$ and $\xi \in [0, T_{\mathrm{f}})$.
In the next section, we present an DA timing acquisition scheme based on the following assumptions: 1) There is no interframe interference, i.e., $\tau_{L-1,0} \leq T_{\mathrm{f}}$. 2) The channel is assumed to be quasi-static, i.e., the channel is constant over a block duration. 3) Since the symbol-level timing offset n_s can be estimated from the symbol-rate samples through the traditional estimation approach, we assumed $n_s = 0$. In this chapter, we focus on acquiring timing with frame-level resolution, which relies on only symbol-rate samples.

3.2 Analysis of symbol-rate sampled data $Y_0[n]$

As shown in Fig. 1, the received signal (6) first passes through a square-law detector. Then, the resultant output is separately correlated with the pre-devised templates $W_0(t)$, $W_1(t)$ and $W_2(t)$, and sampled at nT_{s} which yields $\{Y_0[n]\}_{n=1}^{N-1}$, $\{Y_1[n]\}_{n=1}^{N-1}$ and $\{Y_2[n]\}_{n=1}^{N-1}$. Utilizing these samples, we derive an optimal timing offset estimator $\hat{n}_{\mathrm{f}}$.
In view of (6), the output of the square-law detector is

$$\begin{aligned} R(t) \quad &= \quad r^2(t) = (r_{\mathrm{s}}(t) + n(t))^2 = r_{\mathrm{s}}^2(t) + m(t) \\ &= \quad E_{\mathrm{f}} \sum_{j=0}^{NN_{\mathrm{f}}-1} p_R^2(t - jT_{\mathrm{f}} - a_{\lfloor \frac{j}{N_{\mathrm{f}}} \rfloor} \triangle - \tau_0) + m(t) \end{aligned} \tag{8}$$

where $m(t) = 2r_s(t)n(t) + n^2(t)$. When the template $W(t)$ is employed, the symbol rate sampled data $Y[n]$ is

$$Y[n] \quad = \quad \int_0^{T_s} R(t + nT_s)W(t)dt. \tag{9}$$

Now we derive the decomposition of $Y_0[n]$, i.e., the symbol-rate samples when the template $W_0(t)$ defined as

$$W_0(t) \ = \ \sum_{k=0}^{N_f-1} w(t - kT_f), \ w(t) = \begin{cases} 1, & 0 \le t < \frac{T_f}{2} \\ -1, & \frac{T_f}{2} \le t < T_f \\ 0, & \text{others} \end{cases} \tag{10}$$

is employed. Substituting $W_0(t)$ for $W(t)$ in (9), we obtain symbol-rate sampled data $Y_0[n]$. Recalling (5), we can derive the following proposition of $Y_0[n]$.

Proposition 1: 1) For $1 \le n < N_0$, $Y_0[n]$ can be expressed as

$$Y_0[n] \quad = \quad N_f I_{\xi,0} + M_0[n], \tag{11}$$

2) For $N_0 \le n \le N-1$, $Y_0[n]$ can be represented as

$$Y_0[n] \ = \ \begin{cases} (2\Psi - N_f) I_{\xi,a_{n-1}} + M_0[n], & \xi \in [0, T_\eta) \\ (2\Psi - N_f + 1) I_{\xi,a_{n-1}} + M_0[n], & \xi \in [T_\eta, T_\eta + \frac{T_f}{2}) \\ (2\Psi - N_f + 2) I_{\xi,a_{n-1}} + M_0[n], & \xi \in [T_\eta + \frac{T_f}{2}, T_f) \end{cases} \tag{12}$$

where $\Psi \triangleq n_f - \frac{1}{2}\epsilon$, $\epsilon \in [-\frac{1}{2}, \frac{1}{2}]$ and $T_\eta \in [\frac{T_f}{4}, \frac{T_f}{2}]$. $M_0[n]$ is the sampled noise, and I_{ξ,a_n} is defined as

$$I_{\xi,a_n} \triangleq E_f \int_0^{T_f} \sum_{m=0}^{2} p_R^2(t + mT_f - a_n \triangle - \xi) w(t) dt. \tag{13}$$

We prove the Proposition 1 and the fact that the sampled noise $M_0[n]$ can be approximated by a zero mean Gaussian variable in (Xu et al., 2009) in Appendix A and Appendix B respectively. There are some remarks on the Proposition 1:
1) The fact of $a_{n-1} \in \{0, 1\}$ suggests that $I_{\xi,a_{n-1}}$ in (12) is equal to either $I_{\xi,0}$ or $I_{\xi,1}$. Furthermore, $I_{\xi,0}$ and $I_{\xi,1}$ satisfy $I_{\xi,1} = -I_{\xi,0}$ whose proof is contained in *Fact* 1 of Appendix I.
2) Equation (12) suggests that the decomposition of $Y_0[n]$ varies when ξ falls in different subintervals, so correctly estimating n_f need to determine to which region ξ belongs.
3) *Fact* 2 of Appendix A which states

$$\begin{cases} I_{\xi,0} > 0, & \xi \in [0 \ , \ T_\eta) \bigcup [T_\eta + \frac{T_f}{2} \ , \ T_f] \\ I_{\xi,0} < 0, & \xi \in [T_\eta \ , \ T_\eta + \frac{T_f}{2}) \end{cases} \tag{14}$$

suggests that it is possible to utilize the sign of $I_{\xi,0}$ to determine to which subinterval ξ belongs. However, when $I_{\xi,0} > 0$, ξ could belong to either $[0, T_\eta)$ or $[T_\eta + \frac{T_f}{2}, T_f)$. To resolve this difficulty, we introduce the second template $W_1(t)$ in the next section.

3.3 Analysis of symbol-rate sampled data $Y_1[n]$

The symbol-rate sampled data $Y_1[n]$ is obtained when the template $W_1(t)$ is employed. $W_1(t)$ is a delayed version of $W_0(t)$ with the delayed time $T_{\rm d}$ where $T_{\rm d} \in [0\,,\,\frac{T_{\rm f}}{2}]$. Our simulations show that we obtain the similar performance for the different choices of $T_{\rm d}$. For the simplicity, we choose $T_{\rm d} = \frac{T_{\rm f}}{4}$ for the derivation. Thus, we have

$$\begin{aligned} Y_1[n] &= \int_{\frac{T_{\rm f}}{4}}^{T_{\rm s}+\frac{T_{\rm f}}{4}} R(t+nT_{\rm s})W_0(t-\frac{T_{\rm f}}{4})dt \\ &= \int_0^{T_{\rm s}} R(t+nT_{\rm s}+\frac{T_{\rm f}}{4})W_0(t)dt\,. \end{aligned} \tag{15}$$

Then we can derive the following proposition of $Y_1[n]$.

Proposition 2: 1) For $1 \le n < N_0$, $Y_1[n]$ can be expressed as

$$Y_1[n] = N_{\rm f} J_{\xi,0} + M_0[n]\,. \tag{16}$$

2) For $N_0 \le n \le N-1$, $Y_1[n]$ can be decomposed as

$$Y_1[n] = \begin{cases} (2\Psi - N_{\rm f} - 1)J_{\xi,a_{n-1}} + M_1[n], & \xi \in [0, T_\eta - \frac{T_{\rm f}}{4}) \\ (2\Psi - N_{\rm f})J_{\xi,a_{n-1}} + M_1[n], & \xi \in [T_\eta - \frac{T_{\rm f}}{4}, T_\eta + \frac{T_{\rm f}}{4}) \\ (2\Psi - N_{\rm f} + 1)J_{\xi,a_{n-1}} + M_1[n], & \xi \in [T_\eta + \frac{T_{\rm f}}{4}, T_{\rm f}) \end{cases} \tag{17}$$

where $J_{\xi,0}$ satisfies

$$\begin{cases} J_{\xi,0} < 0\,, & \xi \in [0\ ,\ T_\eta - \frac{T_{\rm f}}{4}) \bigcup [T_\eta + \frac{T_{\rm f}}{4}\ ,\ T_{\rm f}) \\ J_{\xi,0} > 0\,, & \xi \in [T_\eta - \frac{T_{\rm f}}{4}\ ,\ T_\eta + \frac{T_{\rm f}}{4})\,. \end{cases} \tag{18}$$

Equation (14) and (18) suggest that the signs of $I_{\xi,0}$ and $J_{\xi,0}$ can be utilized jointly to determine the range of ξ, which is summarized as follows:

Proposition 3: $\xi \in [0, T_{\rm f}]$ defined in (7) satisfies

1. If $I_{\xi,0} > 0$ and $J_{\xi,0} > 0$, then $\xi \in (\,T_\eta - \frac{T_{\rm f}}{4}\,, T_\eta\,)$.
2. If $I_{\xi,0} < 0$ and $J_{\xi,0} > 0$, then $\xi \in (\,T_\eta\,, T_\eta + \frac{T_{\rm f}}{4}\,)$.
3. If $I_{\xi,0} < 0$ and $J_{\xi,0} < 0$, then $\xi \in (\,T_\eta + \frac{T_{\rm f}}{4}\,, T_\eta + \frac{T_{\rm f}}{2}\,)$.
4. If $I_{\xi,0} > 0$ and $J_{\xi,0} < 0$, then $\xi \in (0, T_\eta - \frac{T_{\rm f}}{4}) \cup (T_\eta + \frac{T_{\rm f}}{2}, T_{\rm f})$.

The last case of Proposition 3 suggests that using the signs of $I_{\xi,0}$ and $J_{\xi,0}$ is not enough to determine whether we have $\xi \in (\,0\,, T_\eta - \frac{T_{\rm f}}{4}\,)$ or $\xi \in (\,T_\eta + \frac{T_{\rm f}}{2}\,, T_{\rm f}\,)$. To resolve this difficulty, the third template $W_2(t)$ is introduced. $W_2(t)$ is an auxiliary template and is defined as

$$W_2(t) = \sum_{k=0}^{N_{\rm f}-1} v(t - kT_{\rm f}),\ v(t) = \begin{cases} 1, & T_{\rm f} - 2T_v \le t < T_{\rm f} - T_v \\ -1, & T_{\rm f} - T_v \le t < T_{\rm f} \\ 0, & \text{others} \end{cases} \tag{19}$$

where $T_v \in (0\,,\, T_{\rm f}/10]$. Similar to the proof of (14), we can prove that in this case, either $K_{\xi,0} > 0$ for $0 < \xi < T_\eta - \frac{T_{\rm f}}{4}$ or $K_{\xi,0} < 0$ for $T_\eta + \frac{T_{\rm f}}{4} < \xi < T_{\rm f}$ is valid, which yields the information to determine which region ξ belongs to.

3.4 The computation of the optimal timing offset estimator $\hat{n}_{\mathrm{f}}$

To seek the estimate of n_{f}, we first compute the optimal estimates of $I_{\xi,0}$ and $J_{\xi,0}$ using (11) and (16). Then, we use the estimate $\hat{I}_{\xi,0}$,$\hat{J}_{\xi,0}$ and Proposition 3 to determine the region to which ξ belongs. The estimate $\hat{\Psi}$ therefore can be derived using the proper decompositions of (12) and (17). Finally, recalling the definition in (12) $\Psi = n_{\mathrm{f}} - \frac{\epsilon}{2}$ with $\epsilon \in [-\frac{1}{2}, \frac{1}{2}]$, we obtain $\hat{n}_{\mathrm{f}} = [\hat{\Psi}]$, where $[\cdot]$ stands for the round operation.

According to the signs of $\hat{I}_{\xi,0}$ and $\hat{J}_{\xi,0}$, we summarize the ML estimate $\hat{\Psi}$ as follow:

Proposition 4:

- When $\hat{I}_{\xi,0} > 0$ and $\hat{J}_{\xi,0} > 0$, $\hat{\Psi} = \frac{1}{A} \sum_{n=N_0}^{N-1} [Z_n + N_{\mathrm{f}}(I_{\xi,0}^2 + J_{\xi,0}^2)]$.
- When $\hat{I}_{\xi,0} < 0$ and $\hat{J}_{\xi,0} > 0$, $\hat{\Psi} = \frac{1}{A} \sum_{n=N_0}^{N-1} [Z_n + (N_{\mathrm{f}} - 1) I_{\xi,0}^2 + N_{\mathrm{f}} J_{\xi,0}^2]$.
- When $\hat{I}_{\xi,0} < 0$ and $\hat{J}_{\xi,0} < 0$, $\hat{\Psi} = \frac{1}{A} \sum_{n=N_0}^{N-1} [Z_n + (N_{\mathrm{f}} - 1)(I_{\xi,0}^2 + J_{\xi,0}^2)]$.
- When $\hat{I}_{\xi,0} > 0$ and $\hat{J}_{\xi,0} < 0$,

$$\hat{\Psi} = \begin{cases} \frac{1}{A} \sum_{n=N_0}^{N-1} [Z_n + N_{\mathrm{f}} I_{\xi,0}^2 + (N_{\mathrm{f}} + 1) J_{\xi,0}^2] & , \hat{K}_{\xi,0} > 0 \\ \frac{1}{A} \sum_{n=N_0}^{N-1} [Z_n + (N_{\mathrm{f}} - 2) I_{\xi,0}^2 + (N_{\mathrm{f}} - 1) J_{\xi,0}^2] & , \hat{K}_{\xi,0} < 0 \end{cases}$$

where $A \triangleq 2(N - N_0)(I_{\xi,0}^2 + J_{\xi,0}^2)$ and $Z_n \triangleq Y_0[n] I_{\xi,a_{n-1}} + Y_1[n] J_{\xi,a_{n-1}}$. The procedures of computing the optimal ML estimate $\hat{\Psi}$ in Proposition 4 are identical. Therefore, we only present the computation steps when $\hat{I}_{\xi,0} > 0$ and $\hat{J}_{\xi,0} > 0$.

1) Utilizing (11) and (16), we obtain the ML estimates

$$\hat{I}_{\xi,0} = \frac{1}{(N_0 - 1) N_{\mathrm{f}}} \sum_{n=1}^{N_0 - 1} Y_0[n], \; \hat{J}_{\xi,0} = \frac{1}{(N_0 - 1) N_{\mathrm{f}}} \sum_{n=1}^{N_0 - 1} Y_1[n] . \tag{20}$$

2) From 1) of Proposition 3, it follows $T_\eta - \frac{T_{\mathrm{f}}}{4} < \xi < T_\eta$ when $\hat{I}_{\xi,0} > 0$ and $\hat{J}_{\xi,0} > 0$.

3) According to the region of ξ, we can select the right equations from (12) and (17) as

$$Y_0[n] = (2\Psi - N_{\mathrm{f}}) I_{\xi,a_{n-1}} + M_0[n] \tag{21}$$

$$Y_1[n] = (2\Psi - N_{\mathrm{f}}) J_{\xi,a_{n-1}} + M_1[n] . \tag{22}$$

Thus the log-likelihood function $\ln p(y\,; \Psi, I_{\xi,a_{n-1}}, J_{\xi,a_{n-1}})$ is

$$\sum_{n=N_0}^{N-1} \left\{ [Y_0[n] - (2\Psi - N_{\mathrm{f}}) I_{\xi,a_{n-1}}]^2 + [Y_1[n] - (2\Psi - N_{\mathrm{f}}) J_{\xi,a_{n-1}}]^2 \right\} .$$

It follows the ML estimate $\hat{\Psi} = \frac{1}{A} \sum_{n=N_0}^{N-1} [Z_n + N_{\mathrm{f}}(I_{\xi,0}^2 + J_{\xi,0}^2)]$.

3.5 Simulation

In this section, computer simulations are performed. We use the second-order derivative of the Gaussian pulse to represent the UWB pulse. The propagation channels are generated

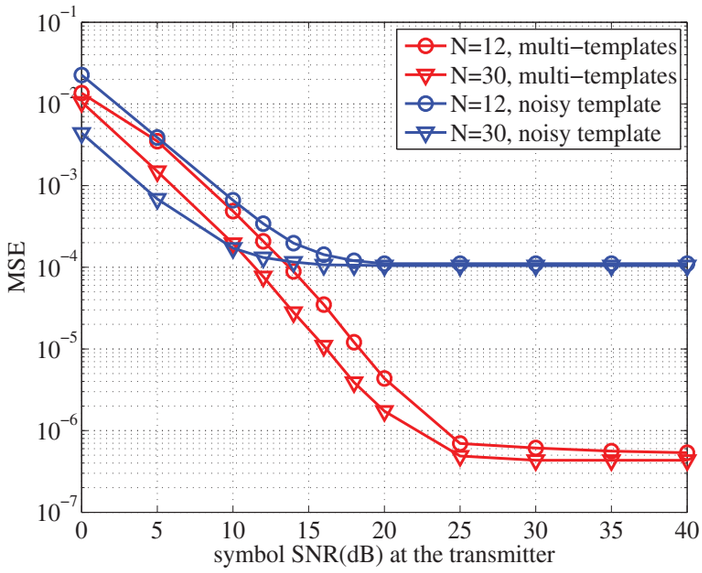

Fig. 2. MSE performance under CM2 with $d = 4m$ ..

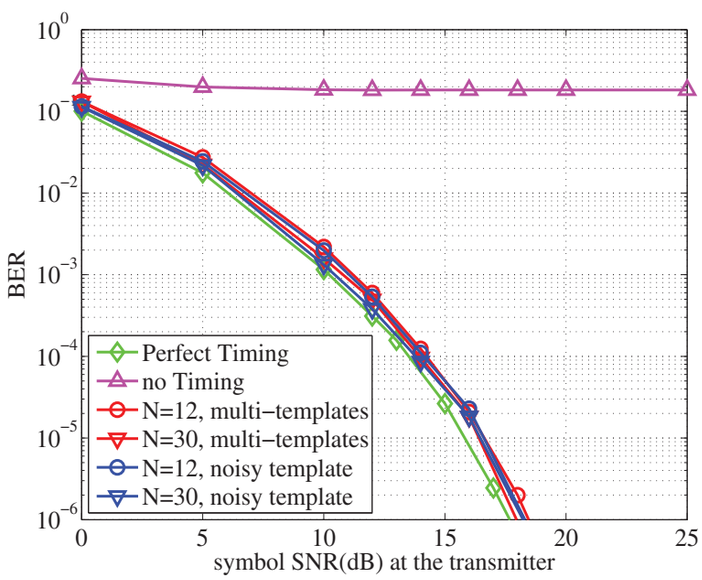

Fig. 3. BER performance under CM2 with $d = 4m$ ..

by the channel model CM2 described in (Foerster, 2003). Other parameters are selected as follows: $T_{\mathrm{p}} = 1\mathrm{ns}$, $N_{\mathrm{f}} = 25$, $T_{\mathrm{f}} = 100\mathrm{ns}$, $T_v = T_{\mathrm{f}}/10$ and the transmitted distance $d = 4m$. In all the simulations, we assume that n_{f} and ξ are uniformly distributed over $[0, N_{\mathrm{f}} - 1]$ and $[0, T_{\mathrm{f}}]$ respectively. To evaluate the effect of the estimate $\hat{n}_{\mathrm{f}}$ on the bit-error-rates (BERs) performance, we assume there is an optimal channel estimator at the receiver to obtain the perfect template for tracking and coherent demodulation. The signal-to-noise ratios (SNRs)

in all figures are computed through E_s/σ_n^2 where E_s is the energy spread over each symbol at the transmitter and σ_n^2 is the power spectral density of the noise.
In Fig. 2 present the normalized mean-square error (MSE:$E\{|(\hat{n}_{\rm f} - n_{\rm f})/N_{\rm f}|^2\}$) of the proposed algorithm in contrast to the approach using noisy template proposed in (Tian & Giannakis, 2005). The figure shows that the proposed algorithm (blue curve) outperforms that in (Tian & Giannakis, 2005) (red curve) when the SNR is larger than 10dB. For both algorithms, the acquisition performance improves with an increase in the length of training symbols N, as illustrated by the performance gap among $N = 12$ and $N = 30$. Fig. 3 illustrates the BER performance for the both algorithms. The BERs corresponding to perfect timing (green curve) and no timing (Magenta curve) are also plotted for comparisons.

4. Low sampling rate channel estimation algorithms

The channel estimation of UWB systems is essential to effectively capture signal energy spread over multiple paths and boost the received signal-to-noise ratio (SNR). The low sampling rate channel estimation algorithms have the merits that can greatly lower the implementation complexity and reduce the costs. However, the development of low sampling rate channel estimation algorithms is extremely challenging. This is primarily due to the facts that the propagation models of UWB signals are frequency selective and far more complex than traditional radio transmission channels.
Classical approaches to this problem are using the maximum likelihood (ML) method or approximating the solutions of the ML problem. The main drawback of these approaches is that the computational complexity could be prohibitive since the number of parameters to be estimated in a realistic UWB channel is very high (Lottici et al., 2002). Other approaches reported are the minimum mean-squared error schemes which have the reduced complexity at the cost of performance (Yang & Giannakis, 2004). Furthermore, sampling rate of the received UWB signal is not feasible with state-of-the-art analog-to-digital converters (ADC) technology. Since UWB channels exhibit clusters (Cramer et al., 2002), a cluster-based channel estimation method is proposed in (Carbonelli & Mitra, 2007). Different methods such as subspace approach (Xu & Liu, 2003), first-order cyclostationary-based method (Wang & Yang, 2004) and compressed sensing based method (Paredes et al., 2007; Shi et al., 2010) proposed for UWB channel estimation are too complex to be implemented in actual systems.
In this section, we develop a novel optimum data-aided channel estimation scheme that only relies on frame-level sampling rate data to derive channel parameter estimates from the received waveform. To begin with, we introduce a set of especially devised templates for the channel estimation. The received signal is separately correlated with these pre-devised templates and sampled at frame-level rate. We show that each frame-level rate sample of any given template can be decomposed to a sum of a frequency-domain channel parameter and a noise sample. The computation of time-domain channel parameter estimates proceeds through the following two steps: In step one, for each fixed template, we utilize the samples gathered at this template and the maximum likelihood criterion to compute the ML estimates of the frequency-domain channel parameters of these samples. In step two, utilizing the computed frequency-domain channel parameters, we can compute the time-domain channel parameters via inverse fast transform (IFFT). As demonstrated in the simulation example,

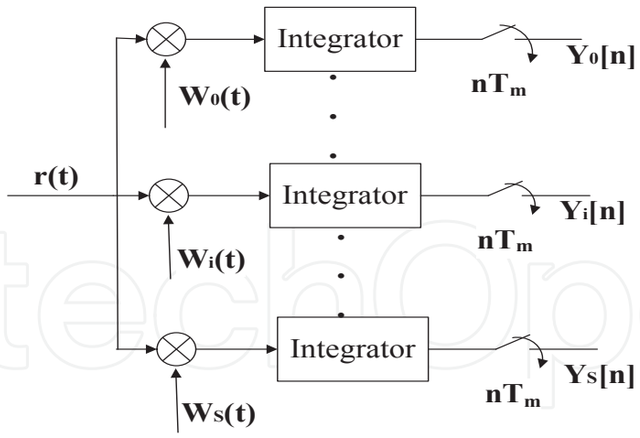

Fig. 4. The block diagram of channel estimation scheme.

when the training time is fixed, more templates used for the channel estimation yield the better (BER) performance.

4.1 The signal model

During the channel estimation process, a training sequence is transmitted. Each UWB symbol is transmitted over a time-interval of T_{s} seconds that is subdivided into N_{f} equal size frame-intervals of length T_{f}, i.e., $T_{\mathrm{s}} = N_{\mathrm{f}} T_{\mathrm{f}}$. A frame is divided into N_{c} chips with each of duration T_{c}, i.e., $T_{\mathrm{f}} = N_{\mathrm{c}} T_{\mathrm{c}}$. A single frame contains exactly one data modulated ultrashort pulse $p(t)$ (so-called monocycle) of duration T_{p} which satisfies $T_{\mathrm{p}} \leq T_{\mathrm{c}}$. The pulse $p(t)$ normalized to satisfy $\int p(t)^2 dt = 1$ can be Gaussian, Rayleigh or other. Then the waveform for the training sequence can be written as

$$s(t) \quad = \quad \sqrt{E_{\mathrm{f}}} \sum_{n=0}^{N_{\mathrm{s}}-1} \sum_{j=0}^{N_{\mathrm{f}}-1} b_n p(t - nT_{\mathrm{s}} - jT_{\mathrm{f}}) \tag{23}$$

where E_{f} represents the energy spread over one frame and N_{s} is the length of the training sequence; b_n denotes data, which is equal to 1 during training phase.
Our goal is to derive the estimate of the channel parameter sequence $\mathbf{h} = [h_0, h_1, \cdots, h_{L-1}]$. Since from the assumption L is unknown, we define a N_{c}-length sequence $\mathbf{p}$ as

$$\mathbf{p} \quad = \quad [h_0, h_1, \cdots, h_{L-1}, h_L, h_{L+1}, \cdots, h_{N_{\mathrm{c}}-1}] \tag{24}$$

where $h_l = 0$ for $l \geq L$. The transmitted signal propagates through an L-path fading channel as shown in (3). Thus the received signal is

$$r(t) = \sqrt{E_{\mathrm{f}}} \sum_{n=0}^{N_{\mathrm{s}}-1} \sum_{j=0}^{N_{\mathrm{f}}-1} \sum_{l=0}^{N_{\mathrm{c}}-1} h_l p(t - nT_{\mathrm{s}} - jT_{\mathrm{f}} - l\,T_{\mathrm{c}}) + n(t) \tag{25}$$

where $n(t)$ is the zero-mean additive white Gaussian noise (AWGN) with double-side power spectral density $\sigma_n^2/2$.

4.2 The choices of templates

In this section, a novel channel estimation method that relies on symbal-level samples is derived. As shown in Fig. 4, the received signal (25) is separately correlated with the pre-devised templates $W_0(t), W_1(t), \cdots, W_S(t)$, and sampled at nT_{m} where sampling period T_{m} is on the order of T_{f}. Let $Y_i[n]$ denote the n-th sample corresponding to the template $W_i(t)$, that is,

$$Y_i[n] = \int_0^{T_{\mathrm{m}}} r(t+nT_{\mathrm{m}})W_i(t)dt \tag{26}$$

with $i = 0, 1, \cdots, S$. Utilizing these samples, we derive the ML estimate of the channel parameter sequence $\mathbf{p}$ in (24).

First we introduce a set of $S+1$ templates used for the channel estimation. The number S is chosen as a positive integer factor of $N_{\mathrm{c}}/2$ by assuming that N_{c} which represents the number of chips T_{c} in each frame is an even number. That is, we have $N_{\mathrm{c}} = 2SM$ with M also being defined as a positive integer factor of $N_{\mathrm{c}}/2$. The i-th template is defined as

$$W_i(t) = \sqrt{E_{\mathrm{f}}} \sum_{k=0}^{N_{\mathrm{o}}-1} \omega_{N_{\mathrm{o}}}^{ik} \left[p(t-kT_{\mathrm{c}}) + p(t-T_{\mathrm{f}}-kT_{\mathrm{c}})\right] \tag{27}$$

with $N_{\mathrm{o}} = 2S = N_{\mathrm{c}}/M$, $\omega_{N_{\mathrm{o}}}^{ik} = e^{-j\frac{2\pi ik}{N_{\mathrm{o}}}}$ and $i \in \{0, 1, \cdots, S\}$. The duration of each template $W_i(t)$ is equal to the sampling period T_{m} which can be expressed as

$$T_{\mathrm{m}} = (N_{\mathrm{c}} + N_{\mathrm{o}})T_{\mathrm{c}} = T_{\mathrm{f}} + N_{\mathrm{o}}T_{\mathrm{c}}. \tag{28}$$

4.3 The computation of the channel parameter sequence $\mathbf{p}$

In this section, we derive the channel estimation scheme that only relies on frame-level sampling rate data. To begin with, let us introduce some notations. Recalling the equation $N_{\mathrm{o}} = N_{\mathrm{c}}/M$ following (27), we divide the N_{c}-length sequence $\mathbf{p}$ into M blocks each of size N_{o}. Therefore, equation (24) becomes

$$\mathbf{p} = [\mathbf{h}_0, \mathbf{h}_1, \cdots, \mathbf{h}_m, \cdots, \mathbf{h}_{M-1}] \tag{29}$$

where the m-th block $\mathbf{h}_m$ is defined as

$$\mathbf{h}_m = [h_{mN_{\mathrm{o}}} \;\; h_{mN_{\mathrm{o}}+1} \;\; \cdots \;\; h_{mN_{\mathrm{o}}+N_{\mathrm{o}}-1}] \tag{30}$$

with $m \in \{0, 1, \cdots, M-1\}$. Let $\mathbf{F}_i$ denote the N_{o}-length coefficient sequence of the i-th template $W_i(t)$ in (27), i.e.,

$$\mathbf{F}_i = [\omega_{N_{\mathrm{o}}}^0 \; \omega_{N_{\mathrm{o}}}^i \; \omega_{N_{\mathrm{o}}}^{2i} \; \cdots \; \omega_{N_{\mathrm{o}}}^{(N_{\mathrm{o}}-1)i}]. \tag{31}$$

The discrete Fourier transform (DFT) of the N_{o}-length sequence $\mathbf{h}_m = [h_{mN_{\mathrm{o}}} \; h_{mN_{\mathrm{o}}+1} \; \cdots \; h_{mN_{\mathrm{o}}+N_{\mathrm{o}}-1}]$ is denoted as

$$\mathbf{H}_m = [H_m^0, H_m^1, \cdots, H_m^i, \cdots, H_m^{N_{\mathrm{o}}-1}] \tag{32}$$

where the frequency-domain channel parameter H_m^i is

$$H_m^i \quad = \quad \mathbf{F}_i \mathbf{h}_m^T = \sum_{k=0}^{N_o-1} \omega_{N_o}^{ik} h_{mN_o+k} \tag{33}$$

with $m \in \{0, 1, \cdots, M-1\}$ and $i \in \{0, 1, \cdots, S\}$.
Our channel estimation algorithm proceeds through the following two steps.

Step 1**:** Utilizing the set of frame-level samples $\{Y_i[n]\}_{n=1}^{N}$ generated from the i-th template, we compute the ML estimates of the frequency-domain channel parameters $\{H_m^i\}_{m=1}^{M}$ for $i \in \{0, 1, \cdots, S\}$. To do this, we show that the samples $\{Y_i[n]\}_{n=0}^{N-1}$ from the i-th template has the following decomposition.

Proposition 1**:** Every sample in the set $\{Y_i[n]\}_{n=0}^{N-1}$ can be decomposed into the sum of a frequency-domain channel parameter and a noise sample, that is,

$$\begin{cases} Y_i[qM] = 2E_f H_0^i + Z_i[qM] \\ Y_i[qM+1] = 2E_f H_1^i + Z_i[qM+1] \\ \qquad \vdots \\ Y_i[qM+m] = 2E_f H_m^i + Z_i[qM+m] \\ \qquad \vdots \\ Y_i[qM+M-1] = 2E_f H_{M-1}^i + Z_i[qM+M-1] \end{cases} \tag{34}$$

where $Z_i[n]$ represents the noise sample. The parameter q belongs to the set $\{0, 1, \cdots, Q-1\}$ with $Q = \lfloor \frac{N}{M} \rfloor$.
Performing ML estimation to the $(m+1)$-th equation in (34) for $q = 0, 1, \cdots, Q-1$, we can compute the ML estimate $\hat{H}_m^i$ for the frequency-domain channel parameter H_m^i as

$$\hat{H}_m^i \quad = \quad \frac{1}{2E_f Q} \sum_{q=0}^{Q-1} Y_i[qM+m] \tag{35}$$

with $m \in \{0, 1, \cdots, M-1\}$ and $i \in \{0, 1, \cdots, S\}$.

Step 2**:** Utilizing the computed frequency-domain channel parameters $\{\hat{H}_m^i\}_{i=0}^{S}$ from the Step 1, we derive the estimate of the time-domain channel sequence $\mathbf{h}_m$ for $m \in \{0, 1, \cdots, M-1\}$. From the symmetry of the DFT, the time-domain channel parameter sequence $\mathbf{h}_m = [h_{mN_o} \; h_{mN_o+1} \; \cdots \; h_{mN_o+N_o-1}]$ is a real valued sequence, which suggests that the DFT of $\mathbf{h}_m$ satisfies

$$H_m^{N_o-i} \quad = \quad (H_m^i)^* \tag{36}$$

with $i \in \{0, 1, \cdots, S\}$ and $S = N_o/2$.
Utilizing equation (36), we obtain the estimate for the N_o-point DFT of $\mathbf{h}_m$ as

$$\hat{\mathbf{H}}_m = [\hat{H}_m^0, \hat{H}_m^1, \cdots, \hat{H}_m^S, (\hat{H}_m^{S-1})^*, \cdots, (\hat{H}_m^2)^*, (\hat{H}_m^1)^*] \tag{37}$$

The estimate of the time-domain channel parameter $\hat{\mathbf{h}}_m$ can be compute via N_o-point IFFT. In view of equation (29), the estimated channel parameter sequence $\mathbf{p}$ in (24) is given by

$$\hat{\mathbf{p}} \quad = \quad [\hat{\mathbf{h}}_0, \hat{\mathbf{h}}_1, \cdots, \hat{\mathbf{h}}_{M-1}]\,. \tag{38}$$

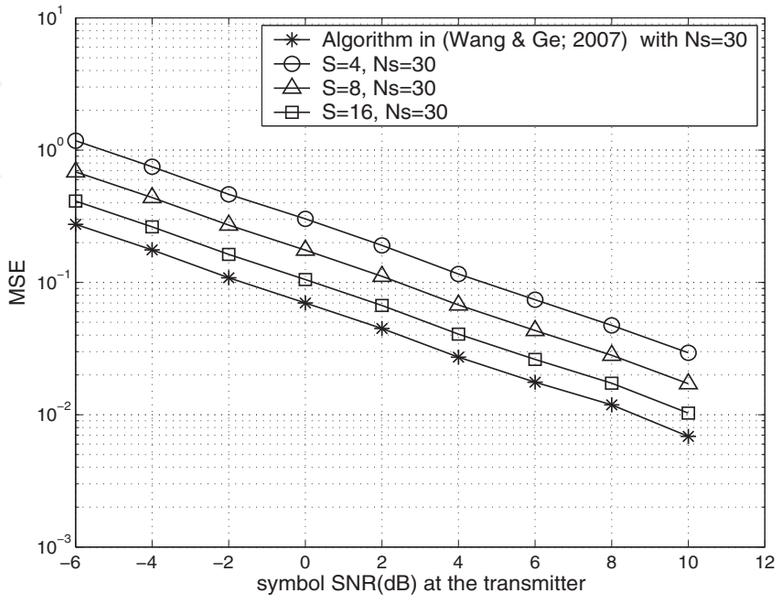

Fig. 5. MSE performance of the algorithm proposed in (Wang & Ge, 2007) and the proposed algorithm with different number of templates ($S = 4\,, 8\,,16$), when the length of the training sequence N_s is $30\,$.

4.4 Simulation

In this section, computer simulations are performed to test the proposed algorithm. The propagation channels are generated by the channel model CM 4 described in (Foerster, 2003)\,. We choose the second-order derivative of the Gaussian pulse as the transmitted pulse with duration $T_p = 1$ns. Other parameters are selected as follows: $T_f = 64$ns, $T_c = 1$ns, $N_c = 64$ and $N_f = 24\,$.

Fig. 5 presents the normalized mean-square error (MSE) of our channel estimation algorithm with different number of templates ($S = 4\,, 8\,, 16$) when the length of the training sequence N_s is $30\,$. As a comparison, we also plot the MSE curve of the approach in (Wang & Ge, 2007) which needs chip-level sampling rate. Fig. 6 illustrates the bit-error-rates (BERs) performance for the both algorithms. The BERs corresponding to the perfect channel estimation (Perfect CE) is also plotted for comparisons. From these figures, the MSE and BER performances of our algorithm improve as the number of templates increases. In particular, as shown in Fig. 5 and Fig. 6, the MSE and BER performances of our algorithm that relies only on the frame-level sampling period $T_f = 64$ns is comparable to that of the approach proposed in (Wang & Ge, 2007) which requires chip-level sampling period $T_c = 1$ns.

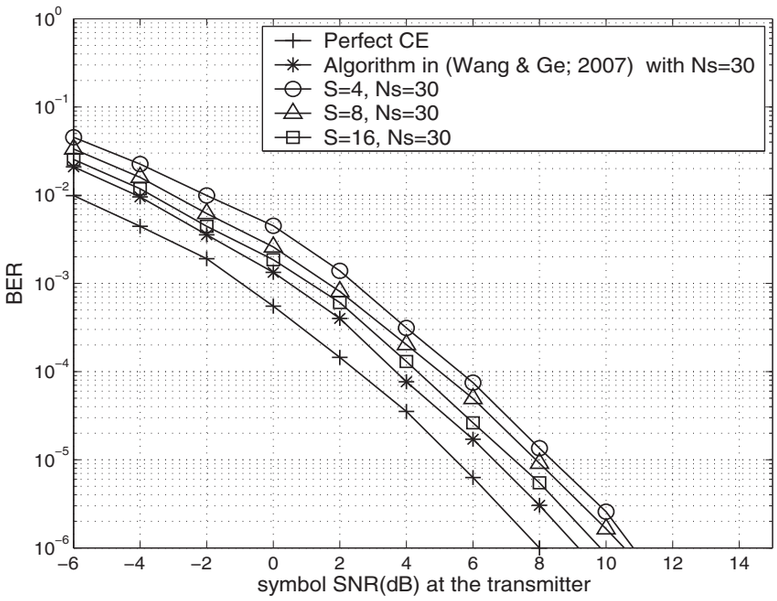

Fig. 6. BER performance of Perfect CE, the algorithm proposed in (Wang & Ge, 2007) and the proposed algorithm with different number of templates ($S = 4, 8, 16$), when the length of the training sequence N_s is 30.

5. Conclusion

In this chapter, we are focusing on the low sampling rate time acquisition schemes and channel estimation algorithms of UWB signals. First, we develop a novel optimum data-aided (DA) timing offset estimator that utilizes only symbol-rate samples to achieve the channel delay spread scale timing acquisition. For this purpose, we exploit the statistical properties of the power delay profile of the received signals to design a set of the templates to ensure the effective multipath energy capture at any time. Second, we propose a novel optimum data-aided channel estimation scheme that only relies on frame-level sampling rate data to derive channel parameter estimates from the received waveform.

6. References

Karaoguz, J. (2001). High-rate wireless personal area networks, *IEEE Commun. Mag.*, vol. 39, pp. 96-102.

Lovelace, W. M. & Townsend, J. K. (2002). The effect of timing jitter and tracking on the performance of impulse radio, *IEEE J. Sel. Areas Commun.*, vol. 20, no. 9, pp. 1646-1651.

Tian, Z. & Giannakis, G. B. (2005). BER sensitivity to mistiming in ultrawideband impulse radios-part I: modeling, *IEEE Trans. Signal Processing*, vol. 53, no. 4, pp. 1550-1560.

Tian, Z. & Giannakis, G. B. (2005). A GLRT approach to data-aided timing acquisition in UWB radios-Part I: Algorithms, *IEEE Trans. Wireless Commun.*, vol. 53,no. 11, pp. IV. 2956-2967.

Yang, L. & Giannakis, G. B. (2005). Timing Ultra-wideband Signals with Dirty Templates,ąś *IEEE Trans. on Commun.*, vol. 53, pp. 1952-1963.

Carbonelli, C. & Mengali, U. (2006). Synchronization algorithms for UWB signals, *IEEE Trans. on Commun.*, vol. 54, no. 2, pp. 329-338.

He, N. & Tepedelenlioglui, C. (2008). Joint Pulse and Symbol Level Acquisition of UWB Receivers, *IEEE Trans. on Wireless Commun.*, vol. 7, no. 1, pp. 6-14.

Carbonelli, C. & Mengali, U. (2005). Low complexity synchronization for UWB noncoherent receivers, in *Proc. 2005 Vehicular Technology Conf.*, vol. 2, pp. 1350-1354.

Furusawa, K.; Sasaki, M.; Hioki, J.; Itami, M.; (2008). Schemes of optimization of energy detection receivers for UWB-IR communication systems under different channel model, *IEEE International Conference on Ultra-Wideband,* pp.157 - 160, Leibniz Universitat Hannover, Germany.

Cheng, X. & Guan, Y. (2008). Effects of synchronization errors on energy detection of UWB signals, *IEEE International Conference on Ultra-Wideband*, pp.161 - 164, Leibniz Universitat Hannover, Germany.

Sasaki, M.; Ohno, J.; Ohno, H.; Ohno, K.; Itami, M. (2010). A study on multi-user access in energy detection UWB-IR receiver, *2010 IEEE 11th International Symposium on Spread Spectrum Techniques and Applications (ISITA)* pp.141 - 146, Taichung, Taiwan.

Xu, W.; Zhao,J.; Wang, D. (2009). A Frame-Level Timing Acquisition Scheme of Ultra-wideband Signals Using Multi-templates, *The 6th International Symposium on Wireless Communication Systems*, pp.61 - 65, Tuscany, Italy.

J. Foerster, Channel modeling sub-commitee report final, *IEEE P802.15-02/490*.

Stoica, L.; Rabbachin, A.; Repo, H.; Tiuraniemi,T.; Oppermann, I. (2005). An ultra-wideband system architecture for tag based wireless sensor networks, *IEEE Trans. on Veh. Technol.*, vol. 54, no. 5, pp. 1632-1645.

Turin, G. L. (1980). Introduction to spread-spectrum antimultipath techniques and their application to urban digital radio, *Proc. IEEE*, vol. 68, pp. 328-353.

Lottici, V; D'Andrea, A. N.; Mengali, U. (2002). Channel estimation for ultra-wideband communications, *IEEE J. Select. Areas Commun.*, vol. 20, no. 9, pp. 1638-1645.

Yang, L. & Giannakis, G. B. (2004). Optimal pilot waveform assisted modulation for ultra-wideband communications, *IEEE Trans. Wireless Commun.*, vol. 3, no. 4, pp. 1236-1249.

Cramer, R. J. M.; Scholtz, R. A.; Win, M. Z. (2002). Evaluation of an ultra wideband propagation channel, *IEEE Trans. Antennas Propagat.*, vol. 50, No. 5.

Carbonelli, C. & Mitra, U. (2007). Clustered ML Channel Estimation for Ultra-Wideband Signals, *IEEE Trans. Wireless Commun.*, vol. 6, No. 7,pp.2412 - 2416.

Paredes, J.L.; Arce, G.R.; Wang, Z. (2007). Ultra-Wideband Compressed Sensing: Channel Estimation, *IEEE Journal of Selected Topics in Signal Processing*, vol. 1, No. 3,pp.383 - 395.

Shi, L.; Zhou, Z.; Tang, L.; Yao, H.; Zhang, J. (2010). Ultra-wideband channel estimation based on Bayesian compressive sensing, *2010 International Symposium on Communications and Information Technologies (ISCIT)*, pp.779 - 782, Tokyo, Japan.

Wang, X. & Ge, H. (2007). On the CRLB and Low-Complexity Channel Estimation for UWB Communications. *IEEE 41st Annual Conference on Information Sciences and Systems*, Baltimore, pp. 151-153.

Xu, Z. & Liu, P. (2003). A subspace approach to blind estimation of ultrawideband channels, in *Proc. IEEE Thirty-Seventh Asilomar Conference on Signals, Systems & Computers*. vol. 2, pp. 1249-1253.

Wang, Z. & Yang, X. (2004). Ultra wide-band communications with blind channel estimation based on first-order statistics, in *Proc. IEEE (ICASSP-04)*. vol. 4, pp. iv-529 - iv-532, Montreal, Canada.

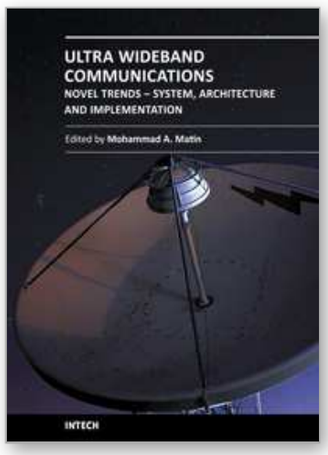

Ultra Wideband Communications: Novel Trends - System, Architecture and Implementation

Edited by Dr. Mohammad Matin

ISBN 978-953-307-461-0
Hard cover, 348 pages
Publisher InTech
Published online 27, July, 2011
Published in print edition July, 2011

This book has addressed few challenges to ensure the success of UWB technologies and covers several research areas including UWB low cost transceiver, low noise amplifier (LNA), ADC architectures, UWB filter, and high power UWB amplifiers. It is believed that this book serves as a comprehensive reference for graduate students in UWB technologies.

InTech Europe
University Campus STeP Ri
Slavka Krautzeka 83/A
51000 Rijeka, Croatia
Phone: +385 (51) 770 447
Fax: +385 (51) 686 166
www.intechopen.com

InTech China
Unit 405, Office Block, Hotel Equatorial Shanghai
No.65, Yan An Road (West), Shanghai, 200040, China
中国上海市延安西路65号上海国际贵都大饭店办公楼405单元
Phone: +86-21-62489820
Fax: +86-21-62489821

IntechOpen